Intravoxel Incoherent Motion Diffusion-Weighted Imaging for Evaluation of the Cell Density and Angiogenesis of Cirrhosis-Related Nodules in an Experimental Rat Model: Comparison and Correlation With Dynamic Contrast-Enhanced MRI

Jiawen Luo, MD,[1] [ID] Kunpeng Zhou, MD,[1] Bin Zhang, PhD,[2] Ning Luo, MD,[1] and Jie Bian, PhD[1]*

Background: Intravoxel incoherent motion diffusion-weighted imaging (IVIM-DWI) and dynamic contrast-enhanced MRI (DCE-MRI) are sensitive imaging modalities for detecting liver lesions, but their value in evaluating cirrhosis-related nodules remains unclear.

Purpose: To investigate whether IVIM-DWI and DCE-MRI can differentiate different types of cirrhosis-related nodules, and whether these modalities can monitor changes in cell density and angiogenesis during the malignant transformation of cirrhosis-related nodules in a rat model

Study Type: Prospective.

Animal Model: Thirty-five male Sprague–Dawley rats with 106 cirrhosis-related nodules (19 regenerative nodules [RNs], 47 dysplastic nodules [DNs], and 40 hepatocellular carcinomas [HCCs]).

Field Strength/Sequence: IVIM-DWI and DCE sequence at 3.0T MRI.

Assessment: IVIM-DWI parameters (D, D*, f, and apparent diffusion coefficient [ADC]) and DCE-MRI parameters (K^{trans}, K_{ep}, and V_e) were calculated by two radiologists using postprocessing software. The "cell density" and "unpaired arterial ratio" were analyzed with a microscope by two pathologists.

Statistical Tests: MRI parameters were compared among the different types of nodules by one-way analysis of variance or the Kruskal–Wallis test. The Pearson correlation test was used to analyze the correlation of MRI parameters with the pathological types of nodules, cell density, and unpaired arterial ratio.

Results: The K^{trans}, K_{ep}, and V_e values of HCCs were significantly higher than those of DNs and RNs. D and ADC values were significantly lower in HCCs than in DNs and RNs. There were moderate positive correlations of K^{trans} with the pathological types of nodules and the unpaired arterial ratio. Moderate negative correlations were observed among D, ADC, and the pathological types of nodules, between D and cell density, and between ADC and cell density.

Data Conclusion: IVIM-DWI and DCE-MRI are valuable in differentiating different types of cirrhotic-related nodules. D and ADC are correlated with changes in cell density during the malignant transformation of cirrhosis-related nodules, while K^{trans} is correlated with increased angiogenesis.

Level of Evidence: 1

Technical Efficacy Stage: 1

HEPATOCELLULAR CARCINOMA (HCC) accounts for more than 90% of liver cancers and is currently the second most lethal tumor globally.[1] The annual mortality rate of HCC has increased significantly over the past two decades.[2] Approximately 80% of HCC cases occur on the background of cirrhosis, which is caused by infection with hepatitis B virus (HBV) and/or hepatitis C virus (HCV).[3] Evidence accumulated in the past decades has confirmed the existence of a multistep carcinogenesis process from regenerative nodules (RNs) to low-grade dysplastic nodules (LGDNs) to high-grade dysplastic nodules (HGDNs) to early hepatocellular carcinoma (eHCC), and finally to the overt HCC in cirrhotic liver.[4,5] Kobayashi et al reported that the transformation rate of RNs to HCC was 12.4% in a 5-year period,[6] and Sato et al found a 50-month transition rate of 40% for DNs to HCC.[7] Hence, to implement appropriate treatment and improve prognosis, it is essential to monitor the progression of cirrhosis-related nodules in patients by noninvasive imaging.

Recently, a considerable number of studies have confirmed that cell density and unpaired arteries are extremely important pathological indicators for the differential diagnosis of RNs, DNs, and HCCs, and that the cell density and the unpaired arteries increase with the gradual transformation of RNs to DNs to HCC.[8–10] Unpaired arteries are small arteries (unaccompanied by a bile duct) that occur outside the original portal tracts, suggesting neoangiogenesis.[8] Kim et al studied the correlation between unpaired arteries and enhanced computed tomography (CT) and found that the number of unpaired arteries in HCCs was related to the degree of arterial phase enhancement.[11] As a noninvasive methodology, dynamic contrast-enhanced magnetic resonance imaging (DCE-MRI) may reflect the neoangiogenesis of cirrhosis-related nodules, since DCE-MRI could reveal the characteristics of vascular permeability, extracellular space, and blood flow of microcirculation perfusion, which are relatively less affected by individual bias and can be evaluated by different hardware settings and programming.[12] In a study of DCE-MRI for the diagnosis of cirrhosis-related nodules, Zhang et al analyzed 45 RNs, 61 DNs, and 37 HCCs and found a positive correlation between each parameter of DCE-MRI and the different cirrhosis-related nodules.[13] To our knowledge, this study is currently the only one to use DCE-MRI to focus on the microcirculatory changes in cirrhotic nodules as they progress to HCC. However, no study has focused on the correlation between DCE-MRI and unpaired arteries of cirrhosis-related nodules.

Diffusion-weighted (DWI) MRI is a functional MRI sequence that is used to describe the Brownian motion of water molecules in biologic tissues. An increase in cell density leads to a decrease in extracellular space, accompanied by a subsequent decrease in mobility, resulting in restricted diffusion.[14] As the most widely used DWI quantitative parameters, the apparent diffusion coefficient (ADC) expresses four main diffusion components, including intracellular diffusion, extracellular diffusion, intravascular diffusion, and transmembranous diffusion. Very few studies have focused on the value of ADC in the differential diagnosis of cirrhotic nodules and HCC, and the results are different or even contradictory. Xu et al studied 40 cases of HCCs and 19 cases of DNs and found that the mean ADC of DNs was significantly higher than that of HCCs.[14] However, another study calculated the ADC value of 8 RNs, 16 DNs, and 32 HCCs of the rat model and found no significant differences between RNs and DNs or between well-differentiated HCC (HCC$_{well}$) and DNs.[15] In an another study of 29 cases of HCC and 24 cases of DN, there was no significant difference in ADC between HCC and DN.[16] We speculated that the conflicting results might be attributed to the "pseudodiffusion" effect caused by non-Brownian motion processes, such as blood flow, which reduces the effectiveness of ADC in reflecting true diffusion information and thus affects the diagnostic efficacy of ADC in the diagnosis of cirrhosis-related nodules. By using the intravoxel incoherent motion model (IVIM), not only can the pure diffusion characteristics (diffusion coefficient, D)—which are more specific than the ADC in reflecting the information of tissue cell density—be measured, but the perfusion characteristics—including the pseudodiffusion coefficient (D*) and perfusion fraction (f)—can also be assessed simultaneously. Such analyses may serve as a surrogate for perfusion information measurement and do not require the injection of contrast agents.[17] To the best of our knowledge, the value of IVIM-DWI in differentiating different types of cirrhosis-related nodules and monitoring the changes in cell density and angiogenesis during the malignant transformation of cirrhosis-related nodules has not been studied.

Therefore, our research explored whether IVIM-DWI and DCE-MRI can differentiate different types of cirrhosis-related nodules and whether these modalities can be used to monitor changes in cell density and angiogenesis during the malignant transformation of cirrhosis-related nodules. Furthermore, we compared the diagnostic efficiency of IVIM-DWI and DCE-MRI for RNs, LGDNs, HGDNs, and HCCs in an experimental rat model.

Materials and Methods
Animal Model
The study was approved by the Institutional Animal Care and Use Committee of the Institutional of Genome Engineered Animal Models for Human Disease (Dalian Medical University, Dalian, China) and was performed in accordance with the National Institutes of Health guidelines for the use of laboratory animals. Fifty male Sprague–Dawley rats (6 weeks old), weighing 120–150 g, were housed in conventional cages under specific pathogen-free environmental conditions and kept at a special room temperature (22 ± 2°C) with a 12-hour lighting time. Cirrhosis-related nodules

were induced with 50 mg/kg DENA (N-nitrosodiethylamine, 0.95 g/ml; Sigma, St. Louis, MO) intragastrically once a week for 10 weeks.[15,18]

MRI

From week 10 to week 20 after the induction of cirrhosis-related nodules by DENA, three to five rats were randomly examined with a 3.0T MR system (Verio; Siemens, Erlangen, Germany) with a four-channel phased-array coil designed for rats (50 mm in diameter, Suzhou Medcoil Healthcare, Suzhou, China) every 7 days (Fig. 1). The rats were fasted for 12 hours and were anesthetized with 40 mg/kg pentobarbital sodium (Shanghai Haling Biological Technology, Shanghai, China) before MRI. To reduce respiratory movement, rats were placed on a plastic holder in the prone position with the liver area in the center of the coil.

All imaging was obtained using the following sequences: transverse T_2-weighted turbo spin-echo (TSE) with fat saturation (repetition time / echo time [TR/TE], 3500/80 msec; flip angle, 150°; echo train length, 7; field of view [FOV], 100 × 80 mm; matrix, 192 × 135; slice thickness, 3 mm; bandwidth, 241 Hz/Pixel; total scan time, 3 min 54 sec). IVIM-DW imaging with nine b values (0, 50, 100, 150, 200, 400, 600, 800, and 1000 sec/mm^2) was performed using a free-breathing single-shot echo-planar imaging pulse sequence with diffusion in three orthogonal directions. The parameters used for this sequence were as follows: TR = 3000 msec, TE = 89 msec; FOV, 90 × 70 mm; section thickness, 3 mm; matrix, 64 × 64; bandwidth, 1012 Hz/Pixel; total scan time 11 minutes 21 seconds. Dynamic contrast-enhanced MRI included four precontrast T_1-weighted measurements (three-dimensional volumetric interpolated breath-hold examination [3D-VIBE]; TR/TE, 8.3/2.3; slice thickness, 3 mm; FOV, 85 × 60 mm;

matrix, 90 × 100; bandwidth 400 Hz/Pixel) with different flip angles (FA of 3°, 6°, 9°, 12°) to obtain data for subsequent baseline T_1 estimation and then followed the dynamic contrast enhancement sequence for T_1 measured with a VIBE sequence. (FA of 12°), 60 continuous measurements lasting for 8 minutes, and each measurement had 20 axial slices. At the end of the precontrast imaging, 0.2 mmol/Kg (0.8 ml/Kg) 50% Gd-DTPA (gadopentetate dimeglumine, Guangzhou Consun Pharmaceutical, Guangzhou China) was administered by manual injection through a tail vein catheter, which was inserted previously (20G, Shanghai, China), followed by a 1-ml saline flush with a maximum period of 5 seconds.

Imaging Analysis

All MRI examinations were independently processed by two radiologists (S.L. and L.J., with 15 years and 10 years of experience in body MRI, respectively) who were blinded to the pathologic results. All parameters of each nodule were measured twice, and their average values were calculated for future statistical analysis to reduce the effect of different region of interest (ROI) delineation and measurement by different observers.

IVIM-DWI. Postprocessing of DWI imaging was performed using homemade software written in MatLab (MathWorks, Natick, MA). First, the estimated signal-to-noise ratio (SNR) was calculated according to formula [1], where the mean SI liver and the mean SI air represent the average SI on liver and air in ROIs at the same imaging level on all b values, respectively; when SNR <5, the data were excluded from the group.[19]
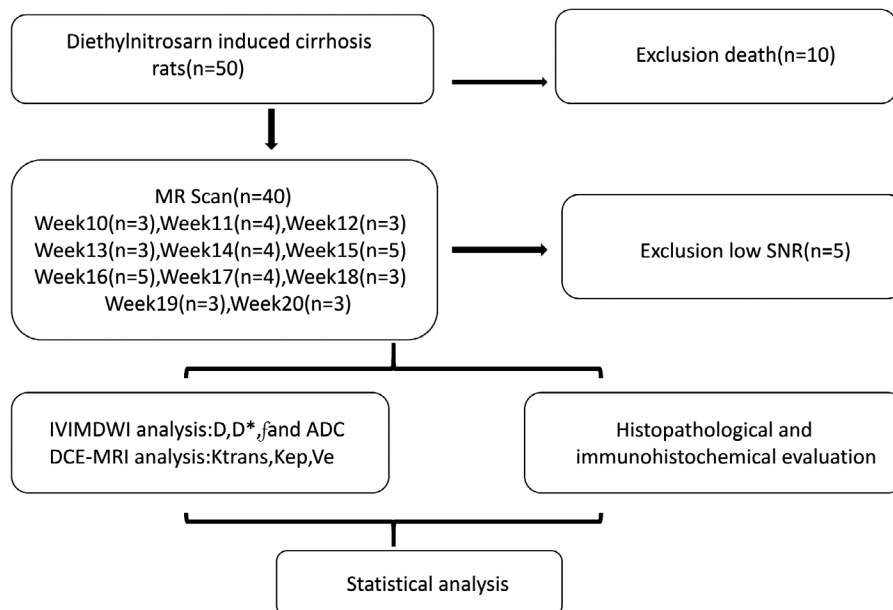

FIGURE 1: The experiment flow chart. Fifty male Sprague–Dawley rats were intragastrically with 5 mg/kg DENA (N-nitrosodiethylamine) once a week for 10–20 weeks. From week 10 to week 20 after the induction of cirrhosis nodules by DENA, three to five rats were examined by MRI once a week. Finally, 35 rats successfully completed the experiment; 10 rats died from the toxic effects of the DENA or from liver cancer and related complications, and 5 rats were excluded because of the low SNR of DWI imaging (<5). Week X = the initial time of gastric administration in rats. K^{trans} = transfer constant; K_{ep} = rate constant; V_e = extravascular extracellular space volume fraction; ADC = apparent diffusion coefficient; D = diffusion coefficient; D* = pseudodiffusion coefficient; f = perfusion fraction.

$$SNR = mean\,SI\,liver\,nodule\,/\,mean\,SI\,air \qquad (1)$$

Second, the DWI data, including all b values, were postprocessed with a nonlinear biexponential fit in MatLab to acquire IVIM-DWI parameters according formula [2],[20] where Sb is the mean signal intensity according to the b value, f is the fraction of diffusion linked to microcirculation (perfusion fraction), D is the diffusion parameter representing pure molecular diffusion, and D* is the diffusion parameter representing blood flow (perfusion-related diffusion).

$$\frac{Sb}{S0} = (1-f)\cdot e^{(-bD)} + f\cdot e^{[-b(D+D^*)]} \qquad (2)$$

The ADC maps were calculated from conventional DWI with b values of 0 and 1000 sec/mm^2 according to formula [3][20]:

$$S = S0\cdot e^{(-b\times ADC)} \qquad (3)$$

Because the T$_2$-weighted image (T$_2$WI_ can distinguish the lesions more clearly, the ROIs for each nodule were drawn on T$_2$WI by two experienced radiologists separately; regions of hemorrhage, degeneration, or necrosis and regions with motion artifact were avoided. Next, the ROIs were copied and pasted onto the IVIM-DWI parameter maps or ADC maps as T$_2$WI as a reference. The D, D*, f, and ADC were evaluated twice, and their average values were calculated.

DCE-MRI. DCE-MRI data were processed using the commercial software Omni-Kinetics (GE Healthcare, Life Science, China). First, motion correction of medical imaging alignment was performed using the nonrigid registration method of the Omni-Kinetics program. The multiple flip angle method was used to perform T$_1$ mapping. Next, the dual-compartment model (dual-input) was used to calculate the kinetic parameters, and the arterial input function (AIF) and the venous input function (VIF) were measured at the abdominal aorta and at the main portal vein, respectively. Then the following maps, including K^{trans}, K$_{ep}$, and V$_e$ were obtained automatically.[21] Next, the ROIs were manually placed on the maximal section of each nodule on T$_2$WI by the two radiologists, carefully avoiding large vessels, necrotic regions, and cystic areas, and then the ROIs were copied and pasted onto the K^{trans} maps, K$_{ep}$ maps, and V$_e$ maps as T$_2$WI as a reference. Finally, each DCE-MRI parameter was evaluated twice, and the mean values were calculated and recorded.

Histopathological and Immunohistochemical Evaluation

All rats were sacrificed by cervical dislocation, and the liver was removed after MRI was completed. To ensure that the pathological tissue corresponded to MRI as accurately as possible, the harvested liver was cut sequentially into 3-mm-thick sections, which approached the MRI transverse plane (Transverse). To determine the nature of the nodules, the harvested nodules were dehydrated, paraffin-embedded, and cut into 4-micron sections, and histological examination was performed with hematoxylin-eosin staining. According to the diagnostic criteria of Pathologic Diagnosis for Early Hepatocellular 2009 and Edmondson-Steiner classification,[8,22] all nodules were histologically diagnosed by two pathologists (W.L.F. and T.J., with 20 years and 10 years of experience in liver pathological diagnosis, respectively) and divided into five groups including RNs, LGDNs, HGDNs, HCC$_{well}$ (Edmondson-Steiner grades 1 and 2) and HCC$_{poor}$ (Edmondson-Steiner grades 3 and 4). To evaluate neoangiogenesis in nodules, liver specimens were also analyzed by immunohistochemical staining using an SMA monoclonal antibody (EnVision, 1:200). The "unpaired arterial ratio" was calculated by two pathologists in all harvest nodules, which was defined as the ratio of the unpaired arteries in the nodule to the normal arteries located in the portal area adjacent to the nodules, and the mean value was calculated for three random fields at ×100 magnification. The "unpaired arteries" were defined as the alpha-smooth muscle actin (α-SMA) positive ring-shaped or tubular structure not accompanied by fibrous tissue and bile ducts on the immunohistological specimens[11,23] The cell density of cirrhosis-related nodules (analyzed using a microscope by two pathologists) was defined as the number of nuclei in nodules divided by the number of nuclei in liver tissues outside nodules (×100).[24] The mean value was counted for three random fields at ×100 magnification, and the average values were recorded.

Statistical Analysis

The IBM SPSS Statistics 20 software (Armonk, NY) was used for statistical computations. Quantitative parameters are expressed as the means ± standard deviation. Data were tested for normality analysis using the Kolmogorov–Smirnov test and then with the Levene test for variance homogeneity analysis. Pearson correlation or Spearman correlation tests were used to analyze the correlation between parameters and the pathological types of nodules, the DWI parameters and the cell density, the DCE-MRI parameters and the "unpaired arterial ratio," and the f and the parameters of DCE-MRI. The correlation coefficient (r) was obtained and the correlation degree was as follows: no relationship if $r < 0.3$, low correlation if $0.3 \leq r < 0.5$, moderate correlation if $0.5 \leq r < 0.8$, excellent correlation if $0.8 \leq r \leq 1$.[25] The one-way analysis of variance (ANOVA) with post-hoc test or nonparametric Kruskal–Wallis test were used to compare parameters from IVIM and DCE-MRI among five groups based on the histopathologic results. The diagnostic performance of IVIM-DWI and DCE-MRI for different types of cirrhosis-related nodules were evaluated by receiver operating characteristic (ROC) analysis. Areas under the ROC curve were compared between IVIM-DWI and DCE-MRI using the Delong test.

Results
Animal Model

Thirty-five rats successfully completed the experiment. Four rats died from the toxic effects of DENA, and six rats died from liver cancer and related complications, such as poor tolerance to anesthesia. Five rats were excluded because of low SNR (<5). Among the total 106 nodules, which were revealed by MRI study and corresponding pathological examination, we identified 19 cases

of RNs (diameter range 5–9 mm, mean = 6.3 mm), 22 cases of LGDNs (6–10 mm, mean = 6.7 mm), 25 cases of HGDNs (5–11 mm, mean = 7.2 mm), 20 cases of HCC$_{well}$ (diameter range 10–20 mm, mean = 16 mm), and 20 cases of HCC$_{poor}$ (diameter range 15–20 mm, mean = 18.8 mm) (Fig. 1). Among them, the sizes of RN, LGDN, and HGDN were not significantly different. The diameters of HCC were significantly larger than those of DN and RN. The diameters of HCC$_{poor}$ were significantly larger than HCC$_{well}$.

MRI Finding

DCE-MRI. With the increase in nodule malignancy, all the DCE-MRI parameters gradually increased. There was a positive correlation between each parameter of DCE-MRI and the five grade nodules (r_{Ktrans} = 0.742, r_{kep} = 0.332, r_{Ve} = 0.492, all $P < 0.01$). The K^{trans}, K$_{ep}$, and V$_e$ values of all HCC were significantly higher than those of DNs and RNs (all $P < 0.05$; Table 1 and Fig. 2). When the five different types of nodules were compared, the values of K^{trans}, K$_{ep}$, and V$_e$ were significantly higher in HCC$_{poor}$ than in HGDNs, LGDNs, and RNs (both $P < 0.05$). The K^{trans} values were higher in HCC$_{poor}$ than in HCC$_{well}$ ($P = 0.04$). The values of K^{trans} were higher in HCC$_{well}$ than in LGDNs and RNs ($P < 0.05$). The K^{trans} values were higher in HGDNs than in LGDNs ($P < 0.01$). There was no significant difference between HCC$_{well}$ and HGDNs among these parameters (Table 1 and Fig. 2). As a semiquantitative index of DCE-MRI, the RE curves of 80% of HCC$_{poor}$, 60% of HCC$_{well}$, 56% of HGDNs, 26.3% of LGDNs, and no RNs showed sharp rises and falls or rapid rises and slow drops.

IVIM-DWI PARAMETERS. The D values and ADC values decreased with increasing grade of nodule malignancy. Some parameters of IVIM were negatively correlated with those different type nodules (r_D = −0.643, r_{ADC} = −0.592, all $P < 0.01$). The D and ADC values were significantly lower in HCC$_{poor}$ and HCC$_{well}$ than in HGDNs, LGDNs, and RNs ($P < 0.05$). The D and ADC values were significantly lower in HCC$_{poor}$ than in HCC$_{well}$. Only the D values of HGDNs were significantly lower than those of LGDNs among these parameters ($P = 0.03$). The D values and ADC values of HGDNs were lower than those of RNs ($P < 0.01$). The f values of HCC$_{poor}$ and HCC$_{well}$ were higher than those of RNs ($P < 0.05$). There was no significant difference between LGDNs and RNs among these IVIM parameters. Regarding the D* values, there were no significant differences between the nodules (Table 2 and Fig. 3).

ROC ANALYSIS RESULTS. ROC analyses demonstrated that K^{trans} had a higher AUC than D and ADC in the diagnosis of RNs and HGDNs, LGDNs, and HGDNs. For the diagnosis of RNs and HCC$_{well}$, LGDNs and HCC$_{well}$, HCC$_{well}$ and HCC$_{poor}$, D had a higher AUC than ADC, K^{trans}, and K$_{ep}$. For HGDN and HCC$_{well}$, the AUC of D was higher than the ADC, with higher specificity and accuracy but lower sensitivity (Tables 3–5).

Histopathological and Immunohistochemical Findings

RNs showed a well-defined region of parenchyma and rounded margins without cellular atypia and increasing cell density, and the unpaired arteries were almost invisible in RNs. The cell density of LGDNs showed a mild increase, but they displayed no cytologic atypia, and the unpaired arteries were sometimes present in small numbers in LGDNs. The HGDNs showed cytologic atypia and increased cell density (some lesions were more than 2 times higher than the peripheral nontumoral liver), accompanied by an irregular trabecular structure, and a small number of unpaired arteries were seen in HGDNs. The cells in HCC often showed obvious cytologic atypia, increased cell density (usually more than twice the surrounding tissue), and a large number of unpaired arteries, and these pathological changes were more pronounced in

---

TABLE 1. DCE-MRI Parameters and Unpaired Arterial Ratio of the Different Pathological Types of Nodules

Group	K^{trans} (min^{-1})	K$_{ep}$ (min^{-1})	V$_e$	Unpaired arterial ratio
RN (n = 19)	0.092 ± 0.001	0.438 ± 0.007	0.231 ± 0.002	0.031 ± 0.002
LGDN (n = 22)	0.093 ± 0.002	0.449 ± 0.006	0.233 ± 0.001	0.082 ± 0.004
HGDN (n = 25)	0.11 ± 0.003	0.454 ± 0.009	0.234 ± 0.003	0.316 ± 0.013
HCCwell (n = 20)	0.115 ± 0.006	0.478 ± 0.01	0.245 ± 0.007	0.416 ± 0.043
HCCpoor (n = 20)	0.137 ± 0.008	0.501 ± 0.012	0.267 ± 0.008	1.149 ± 0.064

Data are expressed as the mean ± standard deviation
RN = Regenerative nodule; LGDN = Low-grade dysplastic nodule; HGDN = High-grade dysplastic nodule; HCCwell = Well-differentiated hepatocellular carcinoma; HCCpoor = Poorly-differentiated hepatocellular carcinoma; Unpaired arterial ratio = the ratio of the unpaired arteries in the nodule and the normal arteries located in the portal area adjacent to the nodules.
K^{trans} = transfer constant; K$_{ep}$ = rate constant; V$_e$ = extravascular extracellular volume fraction.
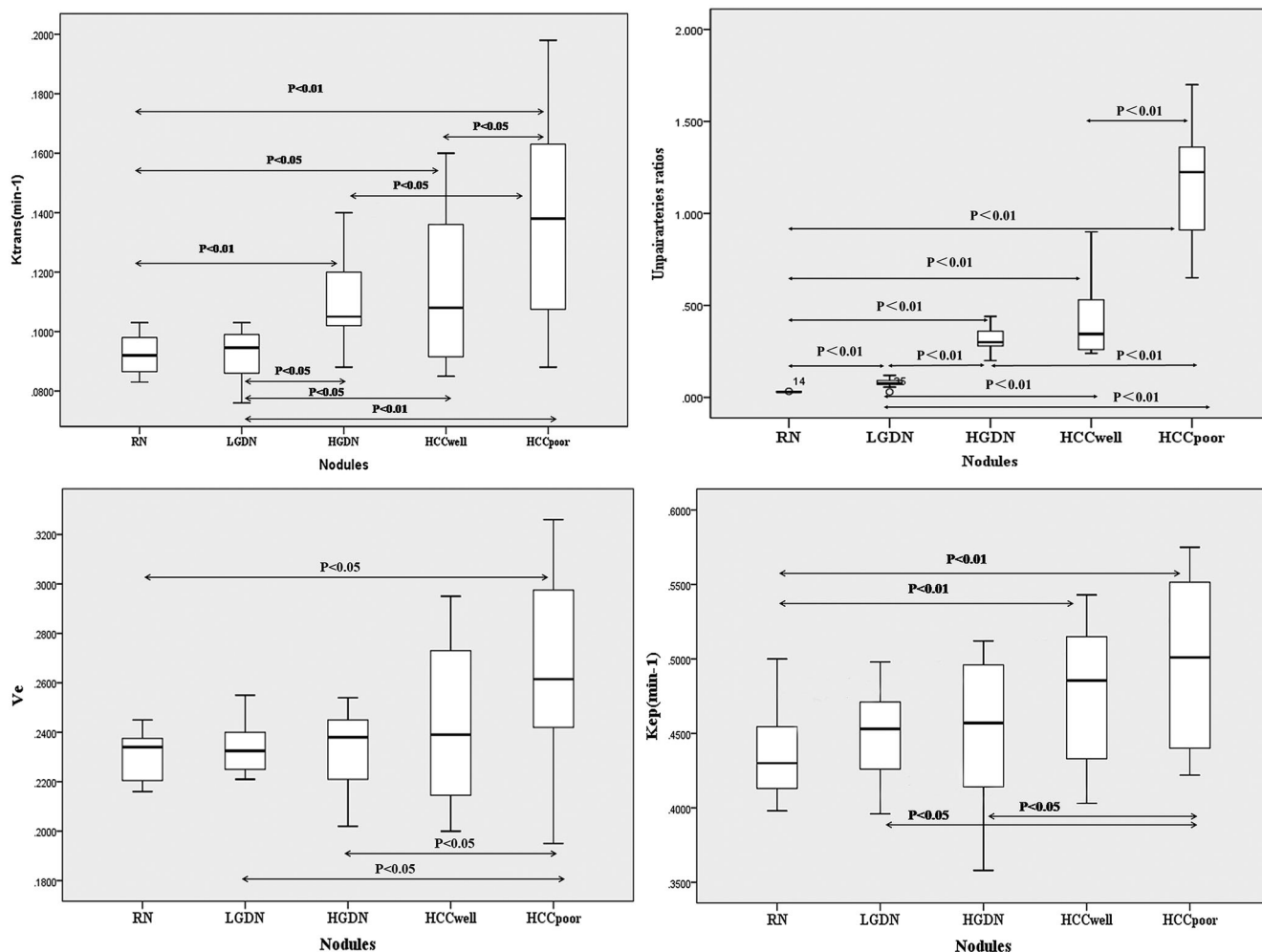
FIGURE 2: Box-and-whisker plots of the DCE-MRI parameters and unpaired arterial ratio in different pathological types of nodules. Significant differences between the different types of nodules are listed in the figure (one-way ANOVA test or Kruskal–Wallis test). RN = regenerative nodules; LGDN = low-grade dysplastic nodules; HGDN = high-grade dysplastic nodules; HCC$_{well}$ = well-differentiated HCC; HCC$_{poor}$ = poorly-differentiated HCC.

HCC$_{poor}$. Quantitative analysis showed that the "unpaired arterial ratio" increased gradually from RNs to LGDNs, HGDNs, HCC$_{well}$, and HCC$_{poor}$, and except for that of HGDNs and HCC$_{well}$, the "unpaired arterial ratio" between different nodules had statistical significance. The cell density also increased gradually with an increase in the malignant degree of the nodules. With the exception of RNs and LGDNs, there were significant differences among other nodules. (Figs. 4–5, Tables 1–2)

Poor to moderate positive correlations were observed between K$_{ep}$ and unpaired arterial ratio ($r = 0.381$, $P < 0.01$), and between K^{trans} and unpaired arterial ratio ($r = 0.531$, $P < 0.01$). There were moderate negative correlations between D and cell density ($r = -0.624$, $P < 0.01$) and between ADC and cell density ($r = -0.526$, $P < 0.01$).

Discussion

The development of most HCCs undergoes a progression from RNs to DNs to DNs with microscopic hepatocellular lesions, then to early HCC, and finally to overt HCC in a cirrhotic liver, and neoangiogenesis plays an important role in carcinogenesis.[3,8,9] In the course of hepatocarcinogenesis, the main form of neoangiogenesis is the gradual establishment of unpaired arteries and the gradual decrease and disappearance of normal arteries,[8] which are substantially different among RNs, LGDNs, HGDNs, and HCCs. To highlight the correlation between neovascularization of cirrhosis-related nodules and DCE-MRI parameters, we arbitrarily used the ratio of unpaired arteries to normal arteries as an indicator of neovascularization of hepatic cirrhosis nodules. Our results showed that the unpaired arterial ratio gradually increased with increasing nodule malignancy, and K^{trans} had a moderate positive correlation with the unpaired arterial ratio. As the most widely accepted DCE-MRI quantitative parameters, K^{trans} describes the transendothelial transport of contrast medium from blood vessels into the extravascular extracellular space depending on the balance between vascular permeability and blood flow in the tissue of interest.[12,26] In the majority of tumors, including HCC, high K^{trans} values represent both high vascular permeability and blood flow, which are

TABLE 2. IVIM-DWI Parameters and Cell Densities of the Different Pathological Types of Nodules

Group	ADC ($\times10\text{-3mm}^2/\text{sec}$)	D ($\times10\text{-3mm}^2/\text{sec}$)	D* ($\times10\text{-3mm}^2/\text{sec}$)	f	Cell densities
RN (n = 19)	1.359 ± 0.028	1.228 ± 0.025	37.147 ± 0.246	19.537 ± 0.165	8.554 ± 0.059
LGDN (n = 22)	1.341 ± 0.025	1.212 ± 0.022	37.089 ± 0.262	19.9 ± 0.186	8.881 ± 0.074
HGDN (n = 25)	1.295 ± 0.021	1.157 ± 0.02	36.88 ± 0.188	20.344 ± 0.190	12.641 ± 0.11
HCCwell (n = 20)	1.212 ± 0.032	1.067 ± 0.031	36.71 ± 0.314	20.705 ± 0.455	15.587 ± 0.218
HCCpoor (n = 20)	1.118 ± 0.03	0.95 ± 0.03	36.58 ± 0.336	20.945 ± 0.453	16.641 ± 0.117

Data are expressed as the mean $\pm$ standard deviation
RN = Regenerative nodule; LGDN = Low-grade dysplastic nodule; HGDN = High-grade dysplastic nodule; HCCwell = Well-differentiated hepatocellular carcinoma; HCCpoor = Poorly-differentiated hepatocellular carcinoma; Cell densities = the ratio of the number of nuclei in nodules and the number of nuclei in liver tissues outside nodules.
ADC = apparent diffusion coefficient; D = diffusion coefficient; D* = pseudodiffusion coefficient; f = perfusion fraction.
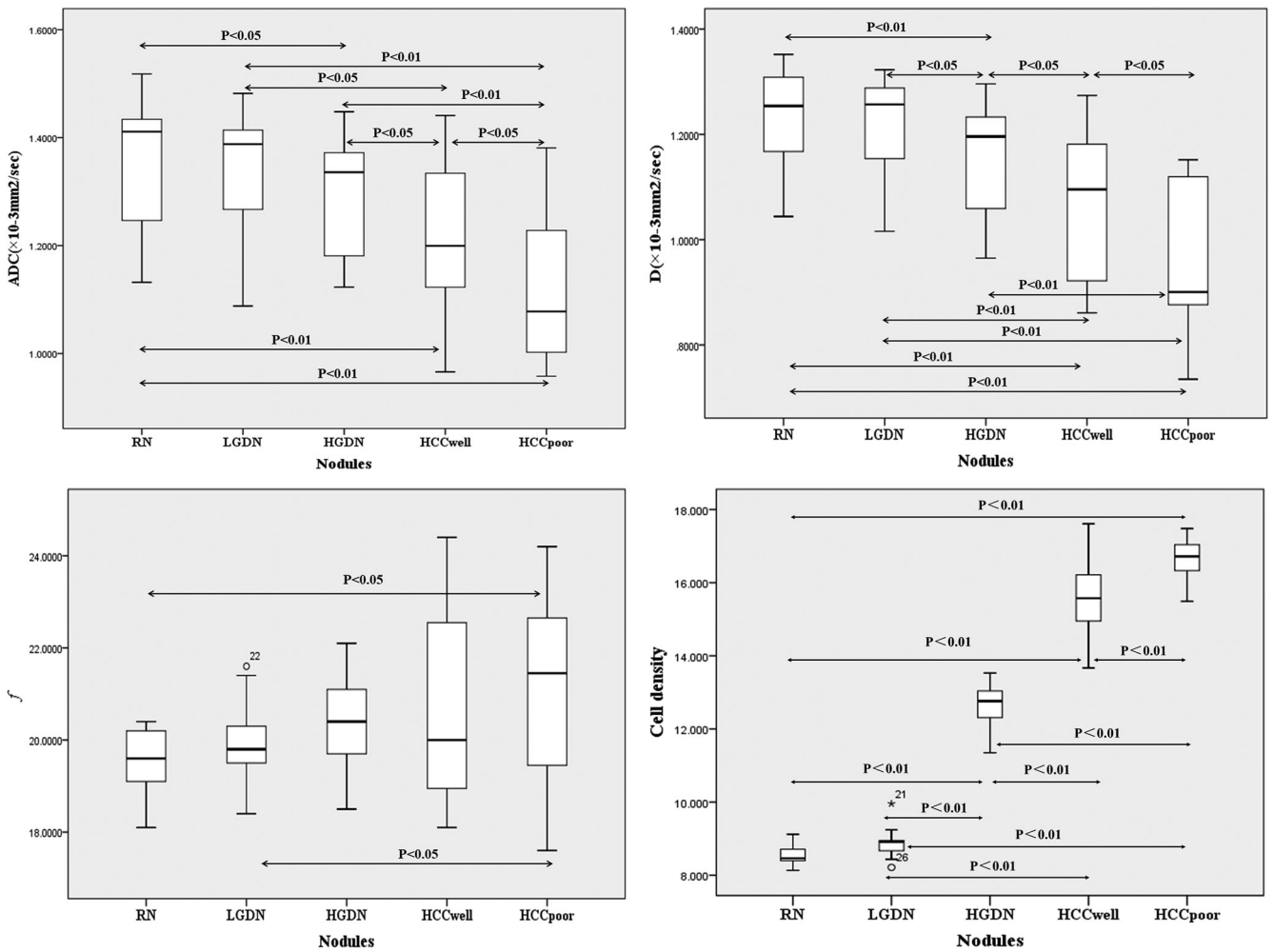

FIGURE 3: Box-and-whisker plots of the IVIM-DWI parameters and cell density in different pathological types of nodules. Significant differences between the different types of nodules are listed in the figure (one-way ANOVA or Kruskal–Wallis test). RN = regenerative nodules; LGDN = low-grade dysplastic nodules; HGDN = high grade dysplastic nodules; HCCwell = well-differentiated HC; HCCpoor = poorly-differentiated HC.

TABLE 3. ROC Analysis Parameters of IVIM and DCE-MRI in the Differential Diagnosis of RN and HGDN, RN, and HCCwell

	RN vs. HGDN			RN vs. HCCwell			
	D	ADC	K^{trans}	D	ADC	K^{trans}	K_{ep}
Cutoff point	1.288	1.424	0.099	1.205	1.339	0.103	0.471
AUROC	0.638	0.585	0.707	0.836	0.782	0.736	0.758
Youden index	0.40	0.20	0.40	0.59	0.53	0.50	0.45
Sensitivity	81.82	77.27	50	0.85	0.85	0.50	0.55
Specificity	57.59	42.11	89.47	0.74	0.69	0.99	0.90
Accuracy	0.71	0.61	0.68	0.80	0.77	0.72	0.69

TABLE 4. ROC Analysis Parameters of IVIM and DCE-MRI in the Differential Diagnosis of LGDN and HGDN, LGDN, and HCCwell

	LGDN vs. HGDN		LGDN vs. HCCwell		
	D	K^{trans}	D	ADC	K^{trans}
Cutoff point	1.244	0.103	1.205	1.339	0.103
AUROC	0.682	0.871	0.811	0.751	0.690
Youden index	0.39	0.64	0.49	0.48	0.50
Sensitivity	0.84	0.64	0.85	0.84	0.50
Specificity	0.55	1.00	0.64	0.63	1.00
Accuracy	0.70	0.77	0.74	0.73	0.71

associated with the degree of malignancy.[13] In our study, the RE curves of 80% of HCC$_{poor}$, 60% of HCC$_{well}$, 56% of HGDNs, 26.3% of LGDNs, and no RNs showed sharp rises and falls or rapid rises and slow drops, which suggests that the blood flow in the nodules increased with the gradual increase in malignancy. In addition, tumor neovascularization such as the formation of

unpaired arteries results in the following physiological changes: increased blood flow and capillary permeability.[11,27,28] Based on the above findings, we speculate that nodular blood flow and vascular permeability increase with the malignant degree of nodules due to the gradual development of unpaired arteries. Several researchers have evaluated the neoangiogenesis of hepatocellular

TABLE 5. ROC Analysis Parameters of IVIM and DCE-MRI in the Differential Diagnosis of HGDN and HCCwell, HCCwell, and HCCpoor

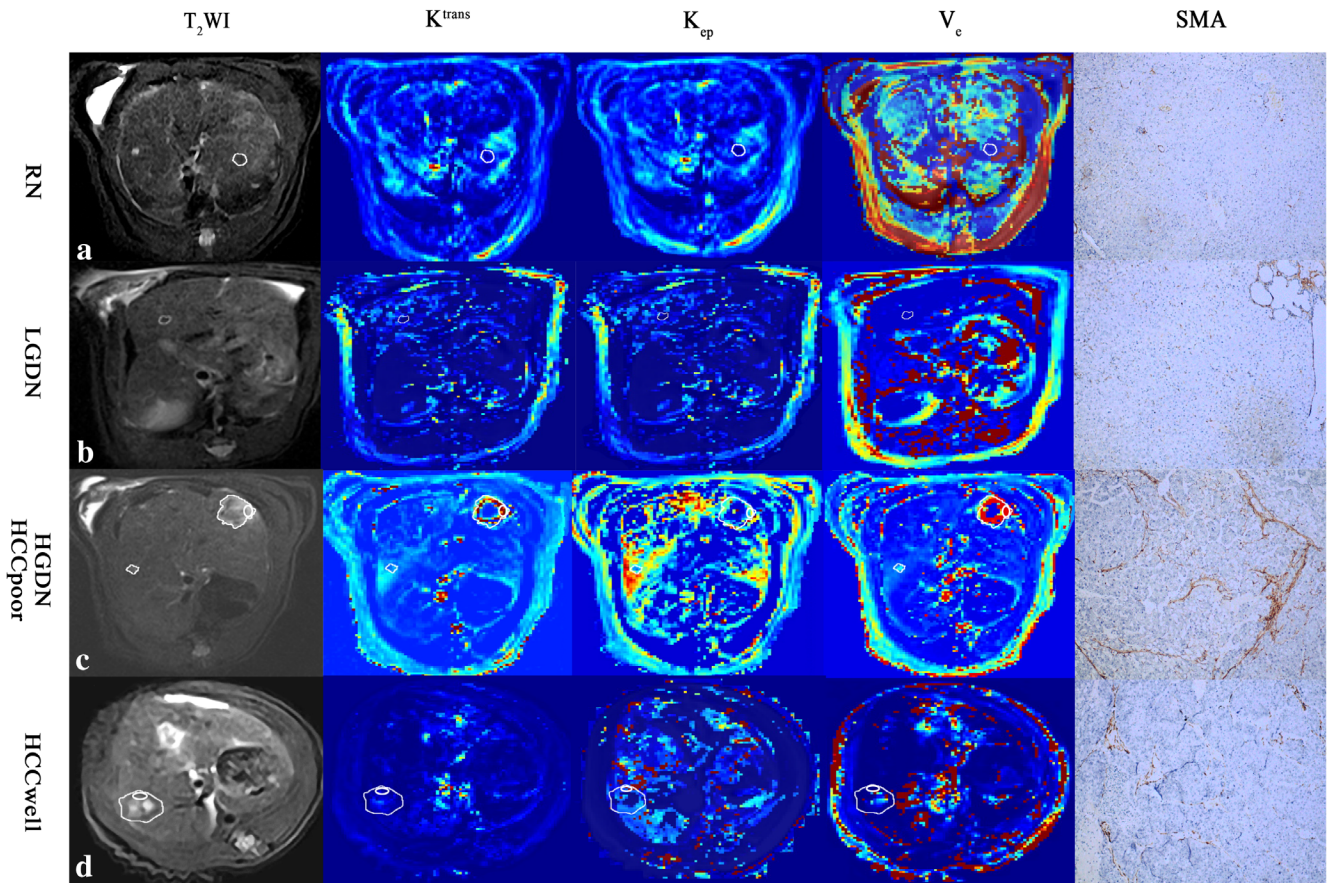|	HGDN vs. HCCwell		HCCwell vs. HCCpoor		
	D	ADC	D	ADC	K^{trans}
Cutoff point	1.033	1.339	0.907	1.12	0.106
AUROC	0.695	0.678	0.725	0.698	0.690
Youden index	0.33	0.31	0.45	0.40	0.30
Sensitivity	0.45	0.85	0.60	0.60	0.80
Specificity	0.88	0.48	0.85	0.80	0.50
Accuracy	0.73	0.67	0.73	0.70	0.72

FIGURE 4: T_2WI, DCE-MRI, and SMA immunohistochemical staining of five different types of cirrhosis-related nodules. Large irregular white circles were used to outline the lesion; in groups c and d, small white oval circles represent the ROI. Group a: the K^{trans} value of RN is 0.091 min^{-1}, the K_{ep} value is 0.435 min^{-1}, and the V_e value is 0.21. Immunohistochemical staining of SMA showed that there were very few unpaired arteries. Group b: the K^{trans}, K_{ep}, and V_e values of LGDN were 0.095 min^{-1}, 0.443 min^{-1}, and 0.225, respectively. Immunohistochemical staining of SMA showed a small number of unpaired arteries. Group c: the smaller lesion was HGDN with K^{trans} 0.113 min^{-1}, K_{ep} 0.446 min^{-1}, and V_e 0.237, and the larger lesion was HCC_{poor}, with K^{trans}, K_{ep}, and V_e values of 0.145 min^{-1}, 0.49 min^{-1}, and 0.276, respectively. SMA staining showed that HCC_{poor} contained a large number of unpaired arteries. In group d: the K^{trans} value of HCC_{well} was 0.121 min^{-1}, the K_{ep} value was 0.477 min^{-1}, and the V_e value was 0.25. SMA staining showed a large number of unpaired arteries.

nodules in the cirrhotic liver with perfusion-weighted MRI or DCE-MRI. Xu et al found that the HCC blood supply was increased, predominantly from the neovascularized hepatic artery, while the blood supply of DNs was the same or lower than that of the surrounding cirrhotic liver.[18] Zhang et al evaluated the angiogenesis of hepatocellular nodules by DCE-MRI and found that the K^{trans} of HCC was significantly higher than that of DNs or RNs, and that K^{trans} had a better diagnostic accuracy than K_{ep} and V_e.[13] Our results are broadly consistent with these findings. ROC analysis showed that K^{trans} had the highest AUC among these DCE-MRI parameters in the differential diagnosis of RNs and HCC, DNs and HCC, and RNs and DNs. However, for the identification of HGDNs and HCC_{well}, the K^{trans} had no diagnostic value. We speculated that this finding may be due to K^{trans} being insufficient to reflect the slight difference in blood flow and vascular permeability between HGDN and HCC_{well}, since our studies showed that there was little difference in the patterns of the RE curve and unpaired artery ratio between HGDNs and HCC_{well}. Previous studies have also found that DN and HCC_{well} have a similar intranodular arterial blood flow and the number of unpaired arteries.[29,30] These studies may support our hypothesis that K^{trans} had no significant difference between HGDNs and HCC_{well} due to relatively similar blood flow and vascular permeability.

An increase in cell density is another characteristic of the malignant transformation of cirrhotic nodules. The cell density increased gradually from RN, LGDN, and HGDN to HCC,[8] which is consistent with our results. Our study showed a moderate negative correlation between D and cell density and between ADC and cell density. These results suggest that DWI, as a promising method that mainly describes the arbitrary random motion of molecules, can reflect the difference in the cell density of these nodules. As the most widely used DWI quantitative parameters, ADC represents the amount of materials that are transported to intracellular, extracellular, intravascular, and transmembranous compartments. However, when the ADC measurements are obtained with b values of less than
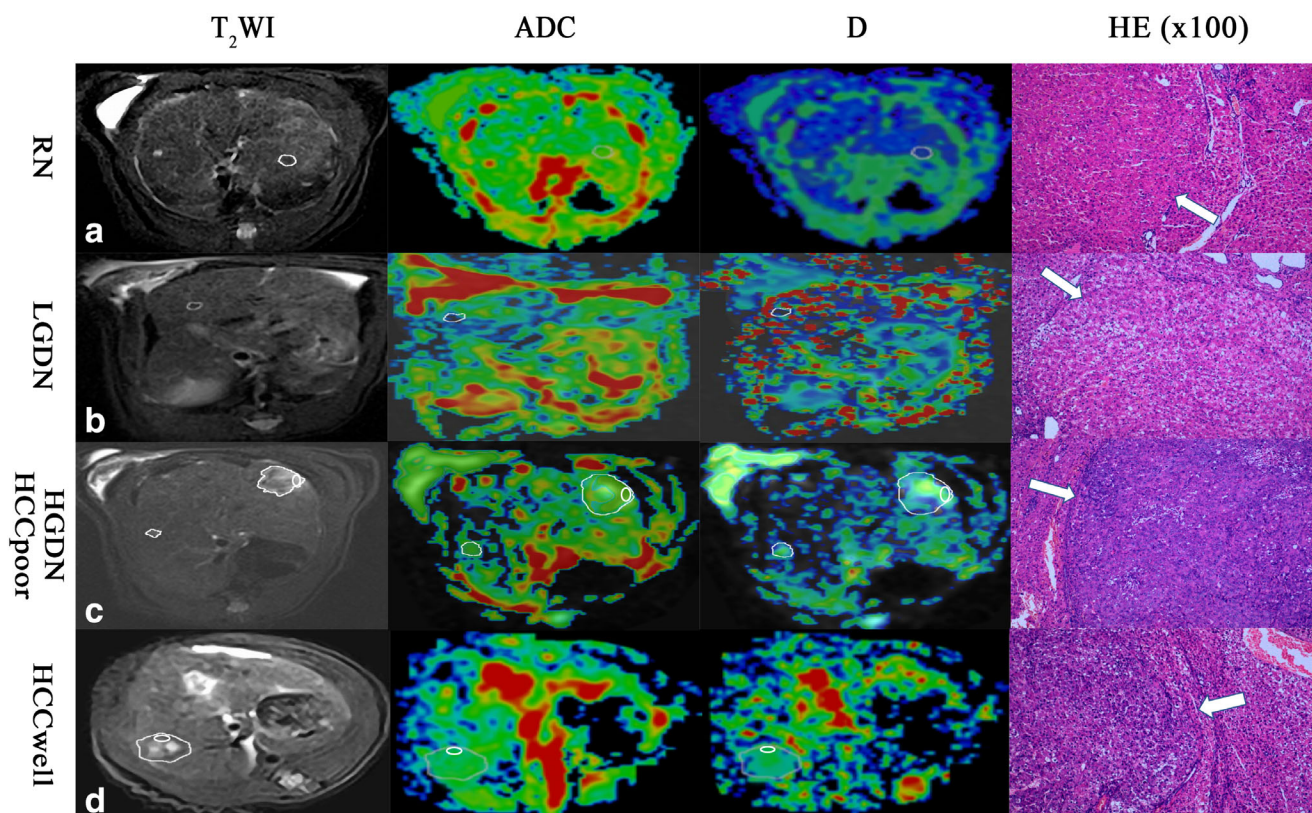
FIGURE 5: Images of T_2WI, IVIM parameters, and hematoxylin-eosin (H&E)-stained samples (original magnification ×100) of five different types of nodules. Large irregular white circles were used to outline the lesion; in groups c and d, small white oval circles represent the ROI. In group a, the ADC and D of RN were 1.367×10^{-3} mm^2/sec and 1.231×10^{-3} mm^2/sec, respectively. H&E staining showed that the cell density in nodules (shown by the white arrow) was similar to that in surrounding liver tissues, and the cell density value was 8.56. In group b, the ADC value of LGDN was 1.321×10^{-3} mm^2/sec, the D value was 1.226×10^{-3} mm^2/sec, and the cell density in the nodules (shown by the white arrow) was higher than that in surrounding liver tissues. The cell density value was 8.88. In group c, the smaller lesions were HGDN, and the ADC and D values were 1.305×10^{-3} mm^2/sec and 1.161×10^{-3} mm^2/sec, respectively. The larger lesion was HCC$_{poor}$, the ADC value was 1.19×10^{-3} mm^2/sec, and the D value was 0.93×10^{-3} mm^2/sec. H&E staining showed that the cell density of HCC$_{poor}$ (as shown by white arrows) was more than 2 times higher than that in surrounding liver tissues, and its cell density value was 16.64. In group d, the ADC and D values of HCC$_{well}$ were 1.232×10^{-3} mm^2/sec and 1.11×10^{-3} mm^2/sec, respectively. H&E staining showed that the cell density value was 15.59.

1000 sec/mm^2, the ADC values mainly reflect the diffusion of water in the extracellular space; that is, the ADC value is mainly affected by the interstitial space, which is accordingly related to cell density.[14,20,24] Our results showed that the ADC decreased with increasing grade of nodule malignancy, except for HGDNs and LGDNs, although we observed that the cell density of HGDNs was higher than that of LGDNs. This finding can be interpreted by the fact that the ADC value contains combined information of pure diffusion (D) and perfusion (f), which may affect the sensitivity of ADC to reflect the cell density difference between HGDNs and LGDNs.[31] Using the IVIM model, the pure diffusion characteristics (high b value regime) can be separated from pseudodiffusion caused by microscopic circulation (low b value regime), which enables calculation of D, D*, and f.[32] Our study showed that D values had a higher diagnostic efficacy than ADC in differentiating RNs from LGDNs, RNs from HCC$_{well}$, LGDNs from HCC$_{well}$, HGDNs from HCC$_{well}$, and HCC$_{well}$ from HCC$_{poor}$. Only

D showed statistical significance among these quantitative parameters in the differential diagnosis of LGDNs and HGDNs. These findings may suggest that D is more sensitive than ADC to changes in cell density. Our results are similar to those of previous reports. Ichikawa et al[33] found that D and ADC in malignant liver lesions were significantly lower than the corresponding values in benign liver lesions, and D was more helpful in differentiating benign from malignant liver lesions than ADC. At the same time, it was observed that the ADC value was always higher than the D value for hypervascular lesions such as hemangioma, while there was no difference between ADC and D for hypovascular lesions such as cysts. These results suggest that with the gradual increase in neovascularization in cirrhosis-related nodules during malignant transformation, the effect of perfusion-related diffusion on ADC may be more obvious.[33] Xu et al found that HCCs have markedly lower ADC values than DNs[14]; Woo et al reported that, compared with low-grade HCC, the D and ADC values are

both significantly lower in high-grade HCC.[31] Our study showed that there was no significant correlation between *f* and DCE-MRI parameters in cirrhosis-related nodules, which was consistent or contrary to previous studies.[34,35] Despite the fact that the reasons for these contradictory results are complex, we believe that IVIM-DWI and DCE-MRI do not share the same conceptual principles. IVIM-DWI is more sensitive to the motion of blood in the direction of the diffusion-encoding gradients, providing information about total blood transit through a voxel including arterial flow, capillary flow, and shunt flow. On the other hand, IVIM-DWI mainly refers to the intravascular compartment movements; however, DCE-MRI includes both intravascular information, extravascular information, and exchange information by continuously tracking contrast for a long time.[34,36]

Our study has some limitations. First, motion artifacts caused by respiratory and cardiac motions would affect DCE-MRI and DWI-MRI. The ECG-gated techniques could effectively reduce cardiac artifacts, but due to the very fast heart rate of rats (~400–600 bpm), this technology was not used in this study. To reduce the impact of respiratory artifacts, we applied three methods: 1) we used pentobarbital for anesthesia, which can inhibit the respiratory movement of rats to a certain extent; 2) the rats were placed in a prone position on a plastic holder with adhesive tape, and the liver area was located at the center of the coil to control respiratory movement; and 3) motion correction of the medical imaging alignment was performed using the nonrigid registration method of the Omni-Kinetics program to reduce movement artifacts. Using the above three methods, the respiratory artifacts of rats were effectively controlled. Second, although the direction of the pathological sections was consistent with the axial DCE-MRI and DWI images as far as possible, and with multiple sequences such as T_2WI as a reference, we are unable to avoid all the nodules completely consistent with the image when analyzing them. Third, some RNs and DNs were relatively small, and the ROI placement may not have been completely accurate. Since cystic degeneration and necrosis are rare in RNs and DNs, we copied the ROI to the parametric maps and encompassed the whole lesion as far as possible, using conventional T_2WI images that could distinguish the lesion more clearly as a reference.15,37

In conclusion, our study indicates that, as noninvasive methods, DCE-MRI and IVIM-DWI are valuable in differentiating different types of cirrhotic nodules. The D and ADC were statistically correlated with the change in cell density during the malignant transformation of cirrhosis-related nodules, while the K^{trans} values were statistically correlated with an increase in angiogenesis. Elevated K^{trans} and reduced D and ADC suggest the malignant transformation of nodules to HCC.

References

1. Global Burden of Disease Liver Cancer C, Akinyemiju T, Abera S, et al. The burden of primary liver cancer and underlying etiologies from 1990 to 2015 at the global, regional, and national level: Results From the Global Burden of Disease Study 2015. JAMA Oncol 2017;3: 1683–1691.

2. European Association for the Study of the Liver. Electronic address, European Association for the Study of the L. EASL Clinical Practice Guidelines: Management of hepatocellular carcinoma. J Hepatol 2018; 69:182–236.

3. Omata M, Cheng AL, Kokudo N, et al. Asia-Pacific clinical practice guidelines on the management of hepatocellular carcinoma: A 2017 update. Hepatol Int 2017;11:317–370.

4. Libbrecht L, Craninx M, Nevens F, Desmet V, Roskams T. Predictive value of liver cell dysplasia for development of hepatocellular carcinoma in patients with non-cirrhotic and cirrhotic chronic viral hepatitis. Histopathology 2001;39:66–73.

5. Borzio M, Bruno S, Roncalli M, et al. Liver cell dysplasia is a major risk factor for hepatocellular carcinoma in cirrhosis: A prospective study. Gastroenterology 1995;108:812–817.

6. Kobayashi M, Ikeda K, Hosaka T, et al. Dysplastic nodules frequently develop into hepatocellular carcinoma in patients with chronic viral hepatitis and cirrhosis. Cancer 2006;106:636–647.

7. Sato T, Kondo F, Ebara M, et al. Natural history of large regenerative nodules and dysplastic nodules in liver cirrhosis: 28-year follow-up study. Hepatol Int 2015;9:330–336.

8. International Consensus Group for Hepatocellular Neoplasia. Pathologic diagnosis of early hepatocellular carcinoma: A report of the International Consensus Group for Hepatocellular Neoplasia. Hepatology 2009;49:658–664.

9. Park YN, Yang CP, Fernandez GJ, Cubukcu O, Thung SN, Theise ND. Neoangiogenesis and sinusoidal "capillarization" in dysplastic nodules of the liver. Am J Surg Pathol 1998;22:656–662.

10. Watanabe S, Okita K, Harada T, et al. Morphologic studies of the liver cell dysplasia. Cancer 1983;51:2197–2205.

11. Kim CK, Lim JH, Park CK, Choi D, Lim HK, Lee WJ. Neoangiogenesis and sinusoidal capillarization in hepatocellular carcinoma: Correlation between dynamic CT and density of tumor microvessels. Radiology 2005;237:529–534.

12. Tofts PS, Brix G, Buckley DL, et al. Estimating kinetic parameters from dynamic contrast-enhanced T(1)-weighted MRI of a diffusable tracer: Standardized quantities and symbols. J Magn Reson Imaging 1999;10: 223–232.

13. Zhang W, Chen HJ, Wang ZJ, Huang W, Zhang LJ. Dynamic contrast enhanced MR imaging for evaluation of angiogenesis of hepatocellular nodules in liver cirrhosis in N-nitrosodiethylamine induced rat model. Eur Radiol 2017;27:2086–2094.

14. Xu PJ, Yan FH, Wang JH, Shan Y, Ji Y, Chen CZ. Contribution of diffusion-weighted magnetic resonance imaging in the characterization of hepatocellular carcinomas and dysplastic nodules in cirrhotic liver. J Comput Assist Tomogr 2010;34:506–512.

15. Xu H, Li X, Xie JX, Yang ZH, Wang B. Diffusion-weighted magnetic resonance imaging of focal hepatic nodules in an experimental hepatocellular carcinoma rat model. Acad Radiol 2007;14:279–286.

16. Inchingolo R, De Gaetano AM, Curione D, et al. Role of diffusion-weighted imaging, apparent diffusion coefficient and correlation with hepatobiliary phase findings in the differentiation of hepatocellular carcinoma from dysplastic nodules in cirrhotic liver. Eur Radiol 2015;25:1087–1096.

17. Le Bihan D, Breton E, Lallemand D, Aubin ML, Vignaud J, Laval-Jeantet M. Separation of diffusion and perfusion in intravoxel incoherent motion MR imaging. Radiology 1988;168:497–505.

18. Xu H, Xie JX, Li X, et al. Perfusion-weighted MRI in evaluating the intranodular hemodynamic characteristics of dysplastic nodules and hepatocellular carcinomas in an experimental rat model. J Magn Reson Imaging 2008;27:102–109.

19. Taouli B, Sandberg A, Stemmer A, et al. Diffusion-weighted imaging of the liver: Comparison of navigator triggered and breathhold acquisitions. J Magn Reson Imaging 2009;30:561–568.

20. Hectors SJ, Semaan S, Song C, et al. Advanced diffusion-weighted imaging modeling for prostate cancer characterization: Correlation with quantitative histopathologic tumor tissue composition—A hypothesis-generating study. Radiology 2018;286:918–928.

21. Yang JF, Zhao ZH, Zhang Y, et al. Dual-input two-compartment pharmacokinetic model of dynamic contrast-enhanced magnetic resonance imaging in hepatocellular carcinoma. World J Gastroenterol 2016;22:3652–3662.

22. Edmondson HA, Steiner PE. Primary carcinoma of the liver: A study of 100 cases among 48,900 necropsies. Cancer 1954;7:462–503.

23. Himeno H, Enzan H, Saibara T, Onishi S, Yamamoto Y. Hitherto unrecognized arterioles within hepatocellular carcinoma. J Pathol 1994;174:217–222.

24. Sugahara T, Korogi Y, Kochi M, et al. Usefulness of diffusion-weighted MRI with echo-planar technique in the evaluation of cellularity in gliomas. J Magn Reson Imaging 1999;9:53–60.

25. Patel J, Sigmund EE, Rusinek H, Oei M, Babb JS, Taouli B. Diagnosis of cirrhosis with intravoxel incoherent motion diffusion MRI and dynamic contrast-enhanced MRI alone and in combination: Preliminary experience. J Magn Reson Imaging 2010;31:589–600.

26. Michoux N, Huwart L, Abarca-Quinones J, et al. Transvascular and interstitial transport in rat hepatocellular carcinomas: Dynamic contrast-enhanced MRI assessment with low- and high-molecular weight agents. J Magn Reson Imaging 2008;28:906–914.

27. Passe TJ, Bluemke DA, Siegelman SS. Tumor angiogenesis: Tutorial on implications for imaging. Radiology 1997;203:593–600.

28. Knopp MV, Weiss E, Sinn HP, et al. Pathophysiologic basis of contrast enhancement in breast tumors. J Magn Reson Imaging 1999;10:260–266.

29. Tajima T, Honda H, Taguchi K, et al. Sequential hemodynamic change in hepatocellular carcinoma and dysplastic nodules: CT angiography and pathologic correlation. AJR Am J Roentgenol 2002;178:885–897.

30. Ikeda K, Kobayashi M, Saitoh S, et al. Origin of neovascular structure in an early stage of hepatocellular carcinoma: Study of alpha-smooth muscle actin immunohistochemistry in serial thin sections of surgically resected cancer. J Gastroenterol Hepatol 2006;21:183–190.

31. Woo S, Lee JM, Yoon JH, Joo I, Han JK, Choi BI. Intravoxel incoherent motion diffusion-weighted MR imaging of hepatocellular carcinoma: Correlation with enhancement degree and histologic grade. Radiology 2014;270:758–767.

32. Kakite S, Dyvorne HA, Lee KM, Jajamovich GH, Knight-Greenfield A, Taouli B. Hepatocellular carcinoma: IVIM diffusion quantification for prediction of tumor necrosis compared to enhancement ratios. Eur J Radiol Open 2016;3:1–7.

33. Ichikawa S, Motosugi U, Ichikawa T, Sano K, Morisaka H, Araki T. Intravoxel incoherent motion imaging of focal hepatic lesions. J Magn Reson Imaging 2013;37:1371–1376.

34. Hectors SJ, Wagner M, Besa C, et al. Intravoxel incoherent motion diffusion-weighted imaging of hepatocellular carcinoma: Is there a correlation with flow and perfusion metrics obtained with dynamic contrast-enhanced MRI? J Magn Reson Imaging 2016;44:856–864.

35. Chandarana H, Lee VS, Hecht E, Taouli B, Sigmund EE. Comparison of biexponential and monoexponential model of diffusion weighted imaging in evaluation of renal lesions: Preliminary experience. Invest Radiol 2011;46:285–291.

36. Henkelman RM. Does IVIM measure classical perfusion? Magn Reson Med 1990;16:470–475.

37. Roncalli M, Borzio M, Di Tommaso L. Hepatocellular dysplastic nodules. Hepatol Res 2007;37(Suppl 2):S125–134.